THE ASTROPHYSICAL JOURNAL, 374:20–28, 1991 June 10

CORRELATION FUNCTIONS OF MATTER FROM GALAXY ROTATION CURVES

STEFANO BORGANI,[1,2] SILVIO A. BONOMETTO,[3] MASSIMO PERSIC,[1,4] AND PAOLO SALUCCI[1,5]

Received 1989 December 28; accepted 1990 November 2

ABSTRACT

Based on the disk-halo decomposition method introduced by Persic & Salucci, we use 58 spiral rotation curves to measure the galaxy-background correlation function in the range 3–350 kpc (for $H_0 = 50$ km s^{-1} Mpc^{-1}). We find that (1) the two-point function is $\xi(r) \simeq (r_0/r)^{1.76}$, with $r_0 \simeq 7$ Mpc (for $\Omega_0 = 1$), and (2) higher order correlation functions are detected up to the sixth order and are found to fit the hierarchical expression.

Subject headings: dark matter — galaxies: clustering — galaxies: structure

1. INTRODUCTION

Dark matter (DM) has long been recognized as a fundamental component of the internal structure of galaxies (Faber & Gallagher 1979). The overall matter distribution, as revealed dynamically by the observed rotation curves, is strikingly different from the distribution of luminous matter in the optical disk region (e.g., Rubin et al. 1985) and extends out to large radii where no velocity falloff is observed (e.g., Bosma 1981; Begeman 1988; Carignan & Freeman 1988; Carignan, Sancisi, & van Albada 1988). Therefore huge amounts of matter, not traced by light, dominate the overall dynamics and structure of galaxies. One may then naturally expect a link between internal galaxy structure and background matter statistics, as suggested by Peebles (1980, 1986).

In order to study the statistics of mass distribution on the scale of galaxies, a proper general technique for decomposing the masses of spiral galaxies into their luminous and dark components is required. Then the knowledge of the physical parameters of DM in the halos allows one to investigate the correlation properties of matter on galaxy scales over a substantial range of luminosities. This is particularly relevant in connection with biased scenarios of galaxy formation (Kaiser 1984; Politzer & Wise 1984; Jensen & Szalay 1986; Bardeen et al. 1986) which establish precise relations between the clustering properties of dynamical and visible matter.

Until quite recently, however, a general mass decomposition technique was not available, so direct investigations of background statistics could not be attempted. A suitable method, which estimates the DM content of spiral galaxies at the optical disk radius from the profiles of rotation curves, was recently devised by Persic & Salucci (1988, 1990a). Such a method is the key starting point for the present study. Indeed, in a previous paper (Bonometto et al. 1990) we made a preliminary investigation of the galaxy-background correlation functions at short distances, finding that matter and galaxy correlation properties are quite similar.

In this paper, based on a larger sample of 58 galaxies from Persic & Salucci (1990a, b, hereafter PS90) sample, we confirm our previous results and expand the analysis to higher order correlation functions by means of the *moment method* (§ 59 of Peebles 1980; Sharp, Bonometto, & Lucchin 1984). This sample is an extension of the one used by Bonometto et al. (1990) and comprises all nonlocal Sb through Sc galaxies for which high-quality, extended rotation curves were available in the literature by the end of 1988. It spans the magnitude interval $-17.5 \geq M_B \geq -23.2$, disk radii range between 3 and 55 kpc, and peripheral velocities between about 100 and 400 km s^{-1}. In § 2 we briefly review Persic and Salucci's method for the disk-halo decomposition of galaxy rotation curves. Application to the PS90 sample gives mean densities for the individual halos. We then derive the two-point (§ 3) and higher order (§ 4) galaxy-background correlation functions. In § 5, after comparing background and galaxy functions, we test the predictions of the BBGKY equations on high-order correlations with our findings. A summary of results is contained in § 6.

We use value $H_0 = 50$ km s^{-1} Mpc^{-1} for the Hubble constant throughout this paper.

2. DARK MATTER IN SPIRAL GALAXIES

In normal spiral galaxies the optical disk radius, $R_{\rm opt}$, is both the length scale of their luminous mass distribution ($R_{\rm opt}$ is ~ 3 times the scale of the exponential light distribution, see Freeman 1970 and van der Kruit 1987) and a very inner radius where DM affects strongly and systematically the observed dynamics (Rubin et al. 1985; Persic & Salucci 1988, and 1991). For this reason $R_{\rm opt}$ is the appropriate reference radius suitable for studying the statistical properties of DM in the same disk region for all galaxies.

Let us define $V_{\rm opt} = V(R_{\rm opt})$ as the value of the observed velocity at $R_{\rm opt}$, and $V_{h,\rm opt}$ as the halo component of $V_{\rm opt}$; let us also define $M_{\rm disk}$ and $M_{\rm halo}$ as the disk and halo masses inside $R_{\rm opt}$. Since

$$V^2_{h,\rm opt} = V^2_{\rm opt} \frac{M_{\rm halo}}{M_{\rm disk} + M_{\rm halo}}, \tag{2.1}$$

$V_{h,\rm opt}$ is obtained from the observed velocity if the disk-to-halo mass ratio is known. For normal spirals modeled as a spherical dark halo and an exponential thin disk of luminous matter, the

[1] SISSA, International School for Advanced Studies, Strada Costiera 11, I-34014 Trieste, Italy.
[2] INFN, Sezione di Perugia, via A. Pascoli, I-06112 Perugia, Italy.
[3] Dipartimento di Fisica dell' Universitá di Milano, via Celoria 16, 20133 Milano, Italy. Also at INFN, Perugia.
[4] Also Osservatorio Astronomico, via G. B. Tiepolo 11, I-34131 Trieste, Italy.
[5] Also Physics Department, University of Durham, Durham DH1 3LE, England.

disk-to-total mass ratio at R_{opt} is

$$\frac{M_{disk}}{M_{disk}+M_{halo}}=\frac{0.8-\nabla}{0.1\nabla+1.1}, \tag{2.2}$$

where $\nabla=(d\log V)/(d\log R)|_{R_{opt}}$ (see Persic & Salucci 1990a).

Let us now consider the condition of centrifugal equilibrium for the halo at R_{opt}, that is, $M_{halo}=G^{-1}V_{opt}^2R_{opt}$. Then, the volume-averaged density of the spherical halo, $\bar{\rho}_{h,opt}$, is

$$\bar{\rho}_{h,opt}=4\times10^{-27}\left(\frac{V_{h,opt}}{R_{opt}}\right)^2 \text{ g cm}^{-3} \tag{2.3}$$

(velocities are in km s^{-1} and radii in kpc). Therefore, the densities of dark halos are obtained directly from the observed rotation curves. From the data in Table 1 we compute the individual values of $\bar{\rho}_{h,opt}$ for the PS90 sample. Recalling that in a Friedmann-Robertson-Walker (FRW) universe the critical density is $\rho_c=5\times10^{-30}$ g cm^{-3}, we finally obtain

$$\frac{\bar{\rho}_{h,opt}}{\Omega_0\rho_c}=\left(\frac{R_0}{R_{opt}}\right)^{1.76\pm0.12}, \tag{2.4}$$

with $R_0=(8.0\pm1.0)$ Mpc (see Fig. 1).

Equation (2.4) is found in the 3–50 kpc distance range and allows us to estimate the background correlation function on these scales. Despite the remarkable similarity between equation (2.4) and the galaxy function, ξ_{gg}, a direct comparison between the two should be made with some caution, as the latter is known over a different scale range, that is, 20 kpc–20 Mpc (Groth & Peebles 1977; Maddox et al. 1990). Therefore, although we can obtain a valid measure of the matter correlation function already at the optical radius of galaxies, we need to sample the density-radius relation farther out in the halos ($R\gg R_{opt}$) in order to extend its radial overlap with ξ_{gg}.

To this purpose let us *define* an effective halo radius, R_h, as

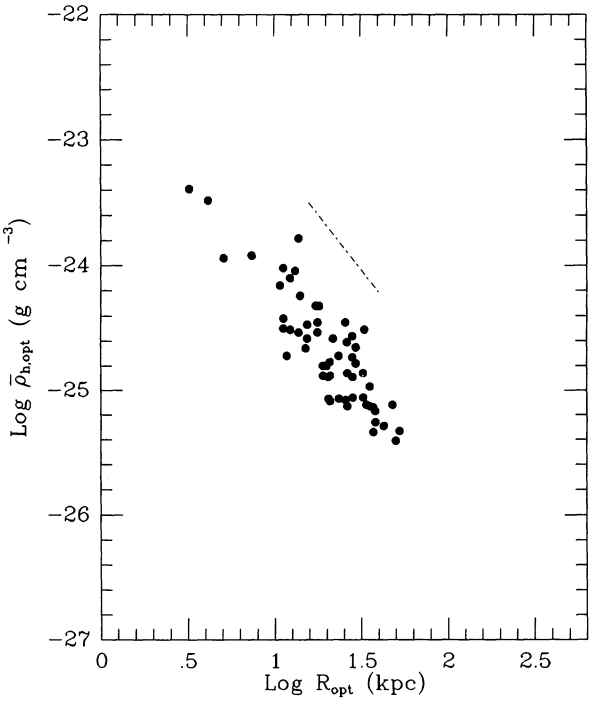

FIG. 1.—Mean halo matter density at the optical disk radius, $\bar{\rho}_{h,opt}$, as a function of the optical disk radius, R_{opt}, for our sample of spiral galaxies. The halo density is considerably higher for optically small, low-luminosity galaxies than for larger, brighter objects. The dashed line indicates the slope $\gamma=1.77$.

TABLE 1

THE SAMPLE OF GALAXIES

Object (1)	M_B (2)	R_{opt} (3)	V_{opt} (4)	M_{disk}/M_{tot} (5)	log $\bar{\rho}_{h,opt}$ (6)
N488	−22.52	33.3	379	0.52	−24.51
N753	−22.60	20.8	209	0.66	−24.77
N1035	−19.69	7.4	138	0.31	−23.92
N1085	−22.55	32.0	310	0.70	−24.86
N1300	−21.47	20.8	200	0.71	−24.88
N1325	−20.87	18.2	209	0.27	−24.32
N1417	−22.28	25.6	308	0.50	−24.45
N1421	−20.80	26.6	225	0.30	−24.61
N1620	−21.90	28.5	265	0.36	−24.56
N2336	−22.50	50.6	252	0.69	−25.41
N2708	−20.60	13.8	283	0.21	−23.78
N2715	−21.21	28.5	177	0.34	−24.89
N2742	−20.54	12.2	190	0.34	−24.10
N2815	−22.00	29.4	286	0.65	−24.78
N2997	−21.19	21.1	160	0.71	−25.09
N2998	−22.00	26.6	214	0.58	−24.86
N3054	−21.63	17.3	239	0.50	−24.32
N3145	−22.58	35.8	276	0.64	−24.97
N3918	−20.60	13.8	158	0.56	−24.53
N3200	−22.87	47.4	288	0.58	−25.12
N3223	−22.64	37.1	255	0.69	−25.14
N3672	−21.75	19.8	190	0.65	−24.80
N3963	−22.37	23.7	177	0.69	−25.07
N3992	−21.70	28.2	277	0.61	−24.73
N4062	−19.50	13.1	201	0.21	−24.04
N4254	−21.51	14.1	204	0.45	−24.24
N4321	−21.53	22.1	227	0.50	−24.58
N4565	−23.20	42.2	254	0.71	−25.29
N4605	−18.59	3.2	95	0.08	−23.39
N4682	−20.85	15.4	179	0.49	−24.47
N4800	−20.00	4.2	165	0.56	−23.48
N5033	−21.30	38.4	219	0.59	−25.17
N5055	−21.55	18.9	200	0.71	−24.80
N5290	−21.51	17.6	220	0.62	−24.53
N5371	−22.60	32.6	240	0.67	−25.06
N5383	−22.50	19.2	209	0.77	−24.88
N5246	−21.24	20.2	157	0.71	−25.07
N5673	−20.50	11.2	125	0.50	−24.50
N5905	−21.84	52.8	250	0.58	−25.33
N5908	−22.00	29.8	350	0.68	−24.65
N7083	−22.40	38.4	223	0.67	−25.26
N7171	−21.25	23.7	227	0.58	−24.72
N7331	−22.40	33.9	226	0.66	−25.12
N7351	−21.14	12.2	180	0.71	−24.51
N7537	−21.23	11.8	137	0.72	−24.72
N7591	−21.21	20.5	195	0.71	−24.89
N7606	−22.54	26.6	257	0.84	−25.13
N7631	−21.17	17.9	208	0.47	−24.45
N7664	−21.60	11.2	183	0.71	−24.42
N7723	−21.57	15.4	209	0.71	−24.58
I467	−20.55	15.0	143	0.51	−24.66
U807	−21.80	37.1	211	0.71	−25.34
U2259	−17.50	5.1	89	0.23	−23.94
U4375	−20.02	10.6	189	0.57	−24.16
U11810	−21.10	28.2	182	0.58	−25.06
U12417	−20.05	11.2	165	0.14	−24.02
U12810	−22.40	35.8	225	0.62	−25.13
WR 66	−20.77	25.6	171	0.62	−25.08

NOTES.—Reported are: Col. (1): name; Col. (2): absolute blue magnitude; Col. (3): optical disk radius (kpc); Col. (4): observed rotation velocity (km s^{-1}) at R_{opt}; Col. (5): disk-to-total mass ratio at R_{opt}; Col. (6): mean halo density (g cm^{-3}) within R_{opt}. Further details on this sample may be found in Persic & Salucci (1990b).

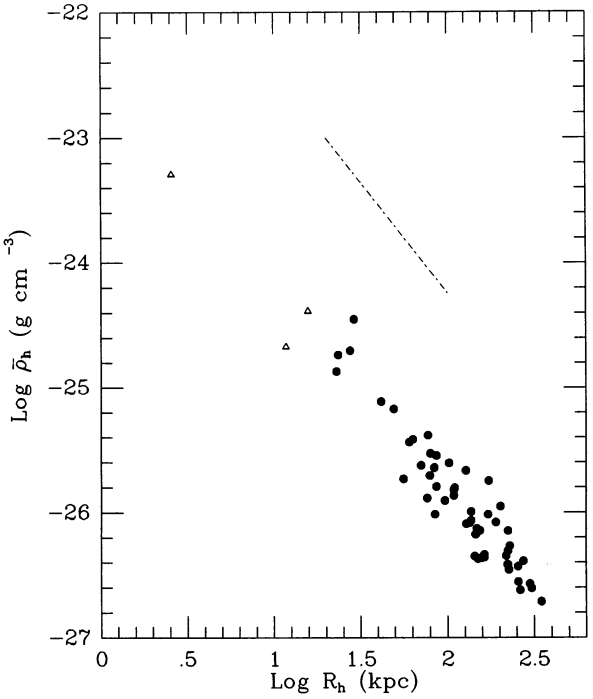

FIG. 2.—Mean halo matter density, $\bar{\rho}_h$, as a function of the effective halo radius, R_h (see text), for the same sample as in Fig. 1. The three triangles represent the galaxies NGC 4605, UGC 2259, and UGC 12417, which are not considered in the moment analysis as they fall in a noncontiguous and insufficiently populated radial bin. In spite of their exclusion from further analyses, the three points fit nicely on the extrapolation of the density-radius correlation to small radii. The dashed line indicates the slope $\gamma = 1.77$.

the radius encompassing an amount of DM η times greater than $M_{\rm disk}$. Consequently the mean halo density at R_h is $\bar{\rho}_h = \eta M_{\rm disk}/[(4/3)\pi R_h^3]$. Observed rotation curves are nearly flat for $R > R_{\rm opt}$, with a value $\simeq V_{\rm opt}$ (e.g., Bosma 1981; Begeman 1988). Accordingly, the condition for centrifugal equilibrium at R_h reads

$$\bar{\rho}_h = 4 \times 10^{-27}\left(\frac{V_{\rm opt}}{R_h}\right)^2 \text{ g cm}^{-3} \qquad (2.5)$$

(same units as in eq. [2.3]). The effective halo radius, R_h appearing in equation (2.5), is not directly observable. It is, however, related to the observable quantities $R_{\rm opt}$ and ∇ through the relation

$$R_h = \eta R_{\rm opt}(0.7 - 0.9\nabla) . \qquad (2.6)$$

Taking $\eta = 10$ (Dekel & Rees 1987; Blumenthal et al. 1984), from the data in Table 1 and equations (2.5) and (2.6) we obtain

$$\frac{\bar{\rho}_h}{\Omega_0 \rho_c} = \left(\frac{R_0}{R_h}\right)^{1.77 \pm 0.09} , \qquad (2.7)$$

with $R_0 = (10.0 \pm 2.5)$ Mpc (see Fig. 2). This implies that the background two-point correlation function, ξ_{bb}, is proportional to the galaxy function, $\xi_{bb} \propto \xi_{\rm gg} \propto r^{-1.77}$, in the distance range 3–350 kpc (see next section). Different choices for η reflect very mildly on R_0, according to $R_0 \propto \eta^{(\gamma-2)/\gamma}$ (this is readily seen from eq. [2.7], recalling that $R_h \propto \eta$ and $\bar{\rho}_h \propto \eta^{-2}$ from eqs. [2.6] and [2.5] above). Also, no variation of the value of γ is induced by different values of η as long as the latter is chosen to be uncorrelated with luminosity.

TABLE 2

MOMENTS OF HALO MASS DISTRIBUTION

Bin limits (kpc) (1)	$\langle M\rangle_k/\tilde{M}_k$ (2)	$R_{2,k}$ (3)	$R_{3,k}$ (4)	$R_{4,k}$ (5)	$R_{5,k}$ (6)	Galaxies per bin (7)
20– 40.....	46400	1.14	1.48	2.09	3.14	4
40– 70.....	10100	1.21	1.63	2.35	3.52	5
70–120.....	4350	1.17	1.57	2.36	3.84	14
120–200.....	1820	1.21	1.77	3.04	5.79	18
200–350.....	808	1.13	1.41	1.95	2.92	14

NOTES.—Moments of the halo mass distribution in the various radial bins. Adimensional quantities $R_{n,k}$ are defined according to eq. (4.8). Col. (1): radial interval of bin; Col. (2): bin-averaged density $\langle M\rangle_k/\tilde{M}_k$, Cols. (3–6): $R_{2,k}$, $R_{3,k}$, $R_{4,k}$, and $R_{5,k}$, respectively; Col. (7): number of galaxies per bin.

In addition to the densities and effective radii shown in Figure 2, we compute other parameters for the extended halos of the PS90 sample. These include the moments of the mass distribution (see Table 2), which will be used in § 3 and § 4 to work out the galaxy-background correlation functions.

3. TWO-POINT FUNCTION ANALYSIS

We consider the *galaxy-background* correlation function $\xi_{\rm gb}(r)$. The expected amount of matter within a sphere of radius R centered on a galaxy (e.g., Peebles 1986) is

$$\langle M\rangle_R = \rho V_R + \rho 4\pi \int_0^R r^2\, dr \xi_{\rm gb}(r) \qquad (3.1)$$

[$V_R = (4/3)\pi R^3$, while $\rho = \rho_c \Omega_0$ is the average matter density]. Assuming

$$\xi_{\rm gb}(r) = (r_0/r)^\gamma$$

(r_0 being the correlation length), in the large-clustering (i.e., $R \ll r_0$) regime, from equation (3.1) we get

$$\frac{\langle M\rangle_R}{\tilde{M}_R} = K_1\, \xi_{\rm gb}(R) , \qquad (3.2)$$

with $\tilde{M}_R = \rho V_R$ and $K_1 = 3/(3-\gamma)$.

If R is interpreted as the halo radius, then by comparing equation (3.2) and equations (2.4) and (2.7), we get

$$R_0 = K_1^{1/\gamma} r_0 . \qquad (3.3)$$

Then we can obtain $\xi_{\rm gb}$ by studying $\bar{\rho}_h = M/V_R$ as a function of the halo size R for each individual galaxy (see Figs. 1 and 2), according to the procedure outlined in § 2. However, the upcoming analyses of higher order correlations (see § 4) require the use of the moment method rather than linear regression. To this purpose we collect the sample galaxies into five bins, each having the same logarithmic amplitude, $\kappa = 1.74$, and a characteristic radius, $r_k = 17.0\kappa$ kpc, which coincides with the logarithmic center of the bin itself (see Table 2). Averaging equation (3.2) over each bin, we obtain

$$\frac{\langle M\rangle_k}{\tilde{M}_k} = K_1 \int_{r_{k,\min}}^{r_{k,\max}} \xi_{\rm gb}(r) p_r\, dr , \qquad (3.4)$$

where p_r is a weight function such that $\int_{r_{k,\min}}^{r_{k,\max}} p_r\, dr = 1$. Taking $p_r \propto r^\alpha$, we get

$$\log \frac{\langle M\rangle_k}{\tilde{M}_k} = \Phi(\alpha, \gamma, r_0, k) \qquad (3.5)$$

TABLE 3

GALAXY-BACKGROUND TWO-POINT CORRELATION FUNCTION

α (1)	r_0(Mpc) (2)	γ (3)
1.....	6.28 ± 0.58	1.71 ± 0.03
2.....	6.44 ± 0.60	1.71 ± 0.03
3.....	6.59 ± 0.62	1.71 ± 0.03

NOTES.—Parameters (logarithmic slope γ and clustering length r_0) of the galaxy-background two-point correlation function. Col. (1): logarithmic slope of power-law weight function; Col. (2) value of r_0 and relative error; Col. (3): value of γ and relative error.

where

$$\Phi(\alpha, \gamma, r_0, k) = \gamma \log \frac{r_0}{r_k} + \log K_1 + \log \frac{\kappa^{\alpha+1-\gamma} - 1}{\kappa^{\alpha+1} - 1} - \log \frac{\alpha + 1 - \gamma}{\alpha + 1} . \quad (3.6)$$

The values of r_0 and γ are found by minimizing the quantity

$$\Sigma_\alpha = \sum_{k=1}^{5} \left[\frac{\Phi(\alpha, \gamma, r_0, k)}{\log (\langle M \rangle_k / \tilde{M}_k)} - 1 \right]^2 . \quad (3.7)$$

We remark that, quite differently from usual correlation analysis of galaxy samples, values relative to different bins are built from different objects, hence are statistically independent.

Best-fit values of r_0 and γ and standard deviations (for $\eta = 10$ and $\Omega_0 = 1$) are reported in Table 3 for different values of α. We find $\gamma = 1.71 \pm 0.03$ independent of α, and $r_0 \simeq (6.5 \pm 0.6)$ Mpc only slightly dependent on α. The same analysis at $R_{\rm opt}$ gives very similar results: $\gamma = 1.72 \pm 0.03$ and $r_0 \simeq (6.4 \pm 0.4)$ Mpc.

A comparison between our results on $\xi_{\rm gb}$ and current results on the two-point *galaxy* function shows that both functions are well modeled by power laws having virtually equal slopes ($\gamma = 1.77 \pm 0.04$ in the case of galaxies; see Pebbles 1980). On the other hand, the *galaxy-galaxy* correlation length, $r_{0,\rm gg}$, is estimated to be $r_{0,\rm gg} \simeq 10$ Mpc (Peebles 1980; Geller 1987; and references therein); therefore it is somewhat greater than the value we find. Thus, our result implies that on scales 3–350 kpc the matter distribution follows the light distribution, possibly except for a moderate bias factor.

4. THE MOMENT METHOD: n-POINT FUNCTION ANALYSIS

It is well known that a Gaussian distribution of density fluctuations originates clustering with vanishing n-point functions ($n > 2$). Detection of n-point functions ($n > 2$) therefore indicates non-Gaussian statistics. This is expected on various grounds. Even starting with a primeval Gaussian distribution (according to canonical inflationary scenarios), subsequent evolution of fluctuations can give rise to non-Gaussianity. For instance, Fry (1984b) shows that, even in the linear regime, self-gravity generates non-Gaussianity. The form he finds for the three-point connected function, at the lowest order in perturbative theory, is

$$\xi^{(3)}_{\rm con}(r_1, r_2, r_3) = Q[\xi^{(2)}(r_1)\xi^{(2)}(r_2) + \xi^{(2)}(r_1)\xi^{(2)}(r_3) + \xi^{(2)}(r_2)\xi^{(2)}(r_3)] . \quad (4.1)$$

Here Q depends in general on the shape of the triangle connecting the three points, but not on the size of the triangle itself (similar expressions for connected n-point functions are also obtained by Fry).

The hierarchical model for n-point functions has similar expressions, in which the n-point correlation function is expressed as a combination of products of $n - 1$ two-point functions,

$$\xi^{(n)}(x_1, \ldots, x_n) = \sum_{n-\text{trees}\, a}^{t_n} Q_{n,a} \sum_{\text{labelings}}^{} \prod_{\text{edges}}^{(n-1)} \xi^{(2)}_{AB} , \quad (4.2)$$

but with constant coefficients (e.g., Fry 1984b). In equation (4.2) distinct *trees* (labeled with $a = 1, \ldots, t_n$) have in general different coefficients Q_a, but configurations differing only in the interchange of labels $1, \ldots, n$ all have same Q_a; AB is a single index identifying links between vertices. The rather cumbersome expression for the number of *trees* t_n with n vertices is a standard result of combinatorial analysis (Riordan 1958; see also Table 1 of Fry 1984b); the total number of labeled trees is n^{n-2} (see eqs. [A1], [A7], [A11], and [A14] for n values up to 6). For $n = 3$, equation (4.2) gives an expression like (4.1), but with constant Q. Similar relations can be found at higher values of n.

From a theoretical point of view, equation (4.2) is a direct output of scale-invariant clustering models (Balian & Schaeffer 1989a, b) and, in the nonlinear clustering regime, is found to be consistent with numerical codes (e.g., Davis et al. 1985; Efstathiou et al. 1988; Valdarnini & Borgani 1990).

Equation (4.2) arises in a natural way also from the solution of the BBGKY equations in the fully relaxed regime ($\xi \gg 1$; e.g., Davis & Peebles 1977; Peebles 1980). The BBGKY solutions provide recurrence relations among different-order $Q_{n,a}$'s whose details depend on the assumptions required to solve the BBGKY hierarchy. For example, Fry (1984a) argued that all the *trees* in equation (4.2) have equal amplitudes,

$$Q_{n,a} = Q_n = \left(\frac{4Q}{n}\right)^{n-2} \frac{n}{2n-2} . \quad (4.3)$$

Hamilton (1988), on the contrary, argues that equation (4.2) can be taken as a solution of the BBGKY hierarchy when only contributions from *snake* graphs are considered, so that

$$Q_{n,\rm snake} = Q^{n-2} , \quad Q_{n,\rm non\text{-}snake} = 0 . \quad (4.4)$$

As we will show in § 5, our results allow a direct comparison between Fry's and Hamilton's realizations of the BBGKY hierarchy.

Let us also outline that, in the frame of *biased* theories of galaxy origin, different expressions are expected to hold for the n-point functions. Assuming Gaussian background fluctuations and identifying observable objects with exceptionally high-density peaks, the Kirchwood superposition holds (see Borgani & Bonometto 1990). Accordingly, the three-point function is

$$\xi^{(3)}_{\rm con}(r_1, r_2, r_3) = Q[\xi^{(2)}(r_1)\xi^{(2)}(r_2) + \xi^{(2)}(r_1)\xi^{(2)}(r_3) + \xi^{(2)}(r_2)\xi^{(2)}(r_3) + \xi^{(2)}(r_1)\xi^{(2)}(r_2)\xi^{(2)}(r_3)] , \quad (4.5)$$

with $Q = 1$ (Jensen & Szalay 1986).

In this section we test the hierarchical expression (4.2) for the n-point correlation functions, up to $n = 6$, from the DM distribution around spiral galaxies, and deduce the numerical value for suitable combinations of the coefficients $Q_{n,a}$ by means of the *moment method* (see Appendix).

Let us consider the joint expected mass value in n infinitesimal volume elements $\delta V_1, \ldots, \delta V_n$ at distances $r_1, \ldots, r_n$ from the center of a galaxy. This can be written as

$$\langle \delta M_1 \ldots \delta M_n \rangle = \rho^n \delta V_1 \ldots \delta V_n [1 + \xi^{(n+1)}_{\text{dis},01\ldots n}] , \quad (4.6)$$

where $\xi^{(n+1)}_{\text{dis},01\ldots n}$ is by definition the *disconnected* correlation function between a galaxy (chosen as the origin of the axes and labeled with zero in the following) and n points lying in the background. The disconnected function contains all the lower order correlation terms that yield the $(n - m)$-point function, when m points are removed, and the *connected* terms that vanish when one point is sufficiently far away.

Integrating n times over a sphere of radius R centered on the galaxy, we obtain

$$\langle M^n \rangle_R = \rho^n \int_0^R \delta V_1 \ldots \int_0^R \delta V_n (1 + \xi^{(n+1)}_{\text{dis},01\ldots n}) . \quad (4.7)$$

We average equation (4.7) over each radial bin and obtain the quantities $\langle M^n \rangle_k$, which generalize the quantity $\langle M \rangle_k$, defined in equation (3.4), to higher correlation order. Due to the large-clustering (e.g., $\xi \gg 1$) regime, in what follows we neglect in equation (4.7) the nonleading contributions from the disconnected terms in $\xi^{(n)}_{\text{dis}}$. We stress that equation (4.7) expresses the n-point correlation functions in terms of the observed mass moments reported in Table 2.

A priori, the hierarchical model leads us to expect that

$$R_{n,k} \equiv \frac{\langle M^n \rangle_k}{\langle M \rangle_k^n} \sim \mathscr{K}_n n^{n-2} Q_{n,a} , \quad (4.8)$$

where $\mathscr{K}_n$ are geometrical factors and n^{n-2} is the total numbers of graphs of order n. The ratio appearing in equation (4.8) does in general depend on the bin index, k, while the right-hand side is strictly constant only in the framework of the hierarchical model. On the other hand, Figure 1 shows that the scatter of masses around $\langle M \rangle_k$ in each radial bin is small, so the adimensional quantities $R_{n,k}$ are roughly constant (see Table 2). This result is in accordance with the hierarchical model expectations, but is in strong disagreement with the Kirchwood model, which implies instead a significative dependence on the label k in the right-hand side of equation (4.8). We can therefore conclude that our data on the DM clustering around galaxies are consistent with the hierarchical model.

Following the procedure outlined in the Appendix, we work out suitable combinations of the hierarchical coefficients (up to the sixth order):

$$Q = 0.43 \pm 0.02 ,$$
$$Q_{4,a} + 0.36 Q_{4,b} = 0.18 \pm 0.02 ,$$
$$Q_{5,a} + 11.43 Q_{5,b} + 9.90 Q_{5,c} = 0.67 \pm 0.11 ,$$
$$Q_{6,a} + 18.06 Q_{6,b} + 13.39 Q_{6,c} + 49.50 Q_{6,d} + 43.59 Q_{6,e} + 52.04 Q_{6,f} = 0.44 \pm 0.12 . \quad (4.9)$$

The signals for the n-point correlations reported in equations (4.9) refer to the halo radius, R_h. We find that at the optical radius, R_{opt}, the signals of the three- and four-point functions are 0.46 ± 0.05 and 0.27 ± 0.09, respectively (the coefficients in the combinations are virtually the same), while no significant signal is found for the five- and six-point functions (cf. the higher scatter in Fig. 1 than in Fig. 2). In equation (4.9) no distinction is made between the terms, entering in $\xi^{(n)}_{\text{dis}}$, which come from galaxy-background and purely background correlations, respectively.

5. DISCUSSION

The range of scales considered in this paper has been partly sampled by studying *galaxy* correlations at short distances. Groth & Peebles (1977) extended the canonical behavior $\xi_{\text{gg}}(r) = (10/r)^{1.77}$ of the two-point function, deduced from the Lick catalog, down to 20 kpc. Gott & Turner (1979) and Lake & Tremaine (1980) claimed the canonical form to hold down to ~ 6 kpc. (Three-dimensional data [Einasto, Klypin, & Saar 1986; de Lapparent, Geller, & Huchra 1987] do not pertain to the relevant scale range). In this paper we measure the correlation function down to 3 kpc directly from the statistical properties of the halo mass excess in galaxies, and find that the canonical behavior extends to such small scales.

A comparison between our results on the two-point galaxy-background correlation functions and the ones on the corresponding galaxy-galaxy function shows that the two functions have strikingly similar slopes. However, if $\Omega_0 = 1$, the respective clustering lengths are different, being $r_{0,\text{gg}}$. If this is the case, the lower value of $r_{0,\text{gb}}$ suggests a bias in the distribution of galaxies. By comparing $r_{0,\text{gg}} \simeq 10$ Mpc and $r_{0,\text{gb}} \simeq 6.5 \Omega_0^{-1/\gamma}$ Mpc, we see that

$$b \equiv \frac{\xi_{\text{gg}}}{\xi_{\text{gb}}} = \left(\frac{r_{0,\text{gg}}}{r_{0,\text{gb}}} \right)^{\gamma} \simeq 2.2 \Omega_0 , \quad (5.1)$$

with a $\sim 20\%$ uncertainty. The above value of the biasing parameter b is consistent with Dekel & Rees's (1987) expectation, based on very different grounds, that $b \sim 2$–3. We emphasize that equation (5.1) is the first *direct* estimate of the biasing parameter b on the scale of galaxies (see also Bonometto et al. 1990), and is uniquely related to our capability of investigating the background (dark) matter statistics.

Any biasing in the distribution of galaxies requires a rescaling of the actual values of our n-point galaxy-background functions by a factor b^{n-1} in order to obtain the corresponding values for the galaxy case. However, due to the very structure of the hierarchical pattern, the coefficients appearing in equation (4.2) are left unchanged by the presence of bias when going from galaxy-background to purely galaxy statistics. Therefore, our outputs on the hierarchical coefficients for higher-order functions can be directly compared with published results coming from number counts, which are hereby briefly summarized.

1. *Three-point function.*—A value $Q \sim 1$ is usually preferred, but values in the range $0.7 \lesssim Q \lesssim 1.3$ have been suggested (Fry 1984b; Peebles & Groth 1975; Groth & Peebles 1977; Sharp et al. 1984; Peebles 1980, and references therein).

2. *Four-point function.*—The determinarton of R_a and R_b was first obtained by Fry & Peebles (1978) on the basis of the two-dimensional Lick sample (Seldner et al. 1977). They found $R_a + \frac{1}{3} R_b = 3.8 \pm 1.2$, or, after smoothing the data, $R_a + \frac{1}{3} R_b = 6.4 \pm 0.6$. However, an independent analysis of the Zwicky sample gives $R_a + \frac{1}{3} R_b = 0.8 \pm 0.6$ (Sharp et al. 1984).

3. *Higher order functions.*—Signals for higher order (up to $n = 8$) functions were recently reported by Szapudi, Szalay, & Boschan (1989) from the analysis of the Lick catalog (Shane & Wirtanen 1967). Those authors found an acceptable agreement with the hierarchical pattern.

We consider purely background functions. By analogy with equation (5.1), the background and galaxy-background two-

TABLE 4

COMBINATIONS OF HIERARCHICAL COEFFICIENTS

Correlation Order	4th	5th	6th
Observations	0.175 ± 0.015	0.675 ± 0.107	0.44 ± 0.12
Fry	0.167 ± 0.015	0.567 ± 0.081	0.70 ± 0.13
Hamilton	0.123 ± 0.011	0.787 ± 0.110	1.49 ± 0.28

NOTES.—The values (4.9) for suitable combinations of hierarchical coefficients $Q_{n,a}$, up to $n = 6$, obtained from data, are compared to the predictions of Fry's (1984) and Hamilton's (1988) solutions of the BBGKY equation, given by eqs. (4.3) and (4.4), respectively.

point functions are related by $\xi_{gb} = b\xi_{bb}$. Consequently, the clustering length of the DM distribution, $r_{0,bb}$, turns out to be

$$r_{0,bb} = b^{-1/\gamma} r_{0,gb} = (4.2 \pm 0.7)\, \Omega_0^{-1/\gamma}\ \text{Mpc} . \qquad (5.2)$$

For $\Omega_0 = 1$ this is about one-half the value of the clustering length of galaxies. We similarly link our n-point (one galaxy and $n-1$ background points) function to its background counterpart (i.e., n background points). Assuming the hierarchical pattern to strictly hold only for the background functions, we find the following signals for the three- and four-point functions:

$$Q^{(b)} = 0.90 \pm 0.15$$
$$R_a^{(b)} + 0.35 R_b^{(b)} = 0.77 \pm 0.25 \qquad (5.3)$$

(due to the structure of the hierarchical pattern, the coefficients appearing in eq. [4.2] are affected by the presence of bias only when going from galaxy-background to purely background statistics). We find no statistically significant signals for the five- and six-point functions.

Finally, the detected signals for higher order functions allow a comparison with Fry's (1982, 1984a) and Hamilton's (1988) hierarchical solutions of the BBGKY equations, that are expressed by equations (4.3) and (4.4), respectively. The results of this comparison are summarized in Table 4, where we report the observational values for the combinations of hierarchical coefficients evaluated at R_h (see eq. [4.9]), together with Fry's and Hamilton's respective predictions (no significant comparison is allowed by the data at R_{opt}). Fry's solution appears here in significantly better agreement with our results, as it predicts values of those combinations remarkably well up to the fifth order, and still within $\sim 1.5\ \sigma$ for the sixth order. In the case of purely background functions, however, we cannot discriminate between Fry's and Hamilton's solutions. In fact, at the fourth order both solutions overlap with our signal.

Comparing our higher order results with the BBGKY predictions is particularly relevant in that the BBGKY equation predicts a hierarchical pattern for higher order correlations only in the statistical equilibrium limit (e.g., Davis & Peebles 1977). Statistical equilibrium is in fact expected on the scale of galaxies, where gravitational relaxation processes have already taken place, while it is hardly expected on the much larger scales of galaxy clustering.

We conclude by pointing out that the PS90 sample, upon which the analysis presented in this paper is based, does not involve any obvious bias other than the requirement that its galaxies should have good quality photometric and kinematic data, to ensure a reliable determination of both the luminous and the total mass distributions. Any possible error coming from inaccuracies in the rotation curve data and data analysis is not included in the formal errors quoted through the paper.

6. CONCLUSION

In this and in our previous paper (Bonometto et al. 1990) we present the first direct study of the correlation properties of (dark) matter on galaxy scales. Our procedure, which is based on the properties of dark halos deduced from the rotation curves of spiral galaxies, allows us to investigate the galaxy-background correlation function with an accuracy comparable, even for a rather limited sample of galaxies, to that achieved by the usual galaxy number-counts correlation analysis applied to large samples. In fact, computing the density of one halo is effectively analogous to counting all the objects within a given distance of a galaxy center; in addition, there is no intersection among the information coming from individual galaxies.

The two-point *galaxy-background* correlation function we obtain is a power law with same slope as the two-point *galaxy* function. A discrepancy between the respective clustering lengths might be indicative of bias. If such is the case, a biasing parameter $b \simeq 2.2\Omega_0$ connects the galaxy and background distributions. The range of scales we sample overlaps widely with the range sampled through galaxy counts, our data extending to yet smaller scales. We find that at such small scales, $\xi(r)$ lies on the extrapolation from its known behavior at larger scales. This seems to indicate that the fluctuation spectrum has the same slope on scales ranging from ~ 20 Mpc down to ~ 3 kpc, despite the expectation that nonlinear evolution and virialization of primeval structure may have modified the (original) fluctuation spectrum on galaxy scales.

As for higher-order correlations, a significant point is that the hierarchical pattern is allowed by observational data up to the sixth order. We also obtain suitable combinations of the hierarchical coefficients $Q_{n,a}$.

As a concluding remark, our approach to the study of matter statistics involves a different physical basis as compared to usual analyses of galaxy clustering. The crucial feature that allows us to link rotation curves and background (dark) matter distribution is our capability of extracting the DM content of spiral galaxies by decomposing the observed rotation curves into their (luminous) disk and dark (halo) components. In our opinion, our results highlight a deep underlying connection between internal structure and large-scale distribution of galaxies.

We thank an anonymous referee for insightful and stimulating comments which helped us to improve considerably the presentation of this work.

APPENDIX

In this Appendix we work out the values of (suitable combinations of) the hierarchical coefficients introduced in equation (4.2) by means of the moment method (see eqs. [4.7], [4.8], and [4.9]).

1. ANALYSIS OF THE THREE-POINT FUNCTION

At the third-order correlation analysis, the hierarchical expression (4.2) contains summations over only one *tree* and three total terms. Thus

$$\xi^{(3)}_{012} = Q(\xi_{01}\,\xi_{02} + \xi_{10}\,\xi_{12} + \xi_{20}\,\xi_{21})\,, \tag{A1}$$

with obvious meaning of the two-point functions' indices. Inserting equation (A1) into equation (4.7) and also taking into account the disconnected terms, it is easy to show that

$$\langle M^2\rangle_R = \rho^2 \int_0^R \delta V_1 \int_0^R \delta V_2[1 + \xi_{r_1} + \xi_{r_2} + \xi_{r_{12}} + Q(\xi_{r_1}\,\xi_{r_2} + \xi_{r_1}\,\xi_{r_{12}} + \xi_{r_2}\,\xi_{r_{12}})]\,, \tag{A2}$$

where $r_{12} = |r_1 - r_2|$. On the other hand,

$$\langle M\rangle^2_R = \rho^2 \int_0^R \delta V_1 \int_0^R \delta V_2(1 + \xi_{r_1} + \xi_{r_2} + \xi_{r_1}\,\xi_{r_2})\,. \tag{A3}$$

By averaging equations (A2) and (A3) over the k-th bin, and including only ξ^2 terms (in the $\xi \gg 1$ regime), we get

$$R_{2,k} = \left(Q + 2Q\,\frac{K_2}{K_1^2}\right) \tag{A4}$$

(here $R_{2,k}$ is defined according to eq. [4.8], taken for $n = 2$). The quantity K_2 is

$$K_2 = \left(\frac{3}{4\pi}\right)^2 \int_0^1 d^3x_1 \int_0^1 d^3x_2 (x_1\,x_{12})^{-\gamma}\,, \tag{A5}$$

while K_1 has been already introduced in § 3. The multiple integral in equation (A5) can be evaluated numerically, and the value it takes for $\gamma = 1.71$ is reported in Table 5. The fit to equation (A4) with the observational $R_{2,k}$ values gives

$$Q = 0.43 \pm 0.02\,. \tag{A6}$$

This value is in very good agreement with the one deduced by Bonometto et al. (1990), but with a smaller statistical error (the error in eq. [A6] corresponds to one formal standard deviation), thanks to the improved statistics of the enlarged PS90 sample.

2. ANALYSIS OF THE FOUR-POINT FUNCTION

In this case, the hierarchical pattern (4.2) provides summations over two different *trees*, corresponding to two different amplitudes $R_a \equiv Q_{3,2}$ and $R_b \equiv Q_{3,1}$, and 16 total terms. Then,

$$\xi^{(4)}_{0123} = R_a[\xi_{01}\,\xi_{12}\,\xi_{23} + \cdots (12 \text{ terms})] + R_b[\xi_{01}\,\xi_{02}\,\xi_{03} + \cdots (4 \text{ terms})]\,. \tag{A7}$$

By averaging equation (4.7) over the kth bin, for $n = 3$ we deduce

$$R_{3,k} = \left[6R_a\left(\frac{K_{3a}}{K_1^3} + \frac{K_2}{K_1^2}\right) + R_b\left(1 + 3\,\frac{K_{3b}}{K_1^3}\right)\right]. \tag{A8}$$

The constants K_{3a} and K_{3b} come from the triple three-dimensional integration in equation (4.7). Their full expressions are:

$$K_{3a} = \left(\frac{3}{4\pi}\right)^3 \int_0^1 d^3x_1 \int_0^1 d^3x_2 \int_0^1 d^3x_3 (x_1\,x_{12}\,x_{23})^{-\gamma}$$

$$K_{3b} = \left(\frac{3}{4\pi}\right)^3 \int_0^1 d^3x_1 \int_0^1 d^3x_2 \int_0^1 d^3x_3 (x_1\,x_{12}\,x_{13})^{-\gamma}\,, \tag{A9}$$

and their numerical values are reported in Table 5.

Substituting the observational values of $R_{3,k}$ in equation (A8) allows us to obtain the value of a suitable combination of R_a and R_b. We find

$$R_a + 0.356R_b = 0.175 \pm 0.015\,, \tag{A10}$$

in good agreement with our earlier result (see Bonometto et al. 1990), but with a consistently smaller error.

3. ANALYSIS OF THE FIVE-POINT FUNCTION

For $n = 5$, equation (4.2) gets rather cumbersome. By using the helpful graph technique (see also Fry 1984b), the contributions from the three different *trees* and 125 total terms can be written as

$$\begin{aligned}\xi^{(5)}_{0\ldots4} = {} & Q_{5,1}[\xi_{01}\,\xi_{02}\,\xi_{03}\,\xi_{04} + \cdots (5 \text{ terms})] \\ & + Q_{5,2}[\xi_{01}\,\xi_{12}\,\xi_{23}\,\xi_{24} + \cdots (60 \text{ terms})] \\ & + Q_{5,3}[\xi_{01}\,\xi_{12}\,\xi_{23}\,\xi_{34} + \cdots (60 \text{ terms})]\,.\end{aligned} \tag{A11}$$

TABLE 5

HIERARCHICAL COEFFICIENTS OF HIGHER ORDER FUNCTIONS

n	Coefficient	Value
2.....	$K_1 = \left(\frac{3}{4\pi}\right) \int_0^1 d^3x_1\, x_1^{-\gamma}$	= 1.326
3.....	$K_2 = \left(\frac{3}{4\pi}\right)^2 \int_0^1 d^3x_1 \int_0^1 d^3x_2 (x_1 x_{12})^{-\gamma}$	= 4.531
4.....	$K_{3a} = \left(\frac{3}{4\pi}\right)^3 \int_0^1 d^3x_1 \int_0^1 d^3x_2 \int_0^1 d^3x_3 (x_1 x_{12} x_{23})^{-\gamma}$	= 8.992
	$K_{3b} = \left(\frac{3}{4\pi}\right)^3 \int_0^1 d^3x_1 \int_0^1 d^3x_2 \int_0^1 d^3x_3 (x_1 x_{12} x_{13})^{-\gamma}$	= 9.696
5.....	$K_{4a} = \left(\frac{3}{4\pi}\right)^4 \int_0^1 d^3x_1 \ldots \int_0^1 d^3x_4 (x_1 x_{12} x_{13} x_{14})^{-\gamma}$	= 18.410
	$K_{4b} = \left(\frac{3}{4\pi}\right)^4 \int_0^1 d^3x_1 \ldots \int_0^1 d^3x_4 (x_1 x_{12} x_{23} x_{24})^{-\gamma}$	= 15.836
	$K_{4c} = \left(\frac{3}{4\pi}\right)^4 \int_0^1 d^3x_1 \ldots \int_0^1 d^3x_4 (x_1 x_{12} x_{13} x_{34})^{-\gamma}$	= 16.762
	$K_{4d} = \left(\frac{3}{4\pi}\right)^4 \int_0^1 d^3x_1 \ldots \int_0^1 d^3x_4 (x_1 x_{12} x_{23} x_{34})^{-\gamma}$	= 11.358
6.....	$K_{5a} = \left(\frac{3}{4\pi}\right)^5 \int_0^1 d^3x_1 \ldots \int_0^1 d^3x_5 (x_1 x_{12} x_{13} x_{14} x_{15})^{-\gamma}$	= 38.245
	$K_{5b} = \left(\frac{3}{4\pi}\right)^5 \int_0^1 d^3x_1 \ldots \int_0^1 d^3x_5 (x_1 x_{12} x_{23} x_{24} x_{25})^{-\gamma}$	= 30.441
	$K_{5c} = \left(\frac{3}{4\pi}\right)^5 \int_0^1 d^3x_1 \ldots \int_0^1 d^3x_5 (x_1 x_{12} x_{13} x_{14} x_{45})^{-\gamma}$	= 34.691
	$K_{5d} = \left(\frac{3}{4\pi}\right)^5 \int_0^1 d^3x_1 \ldots \int_0^1 d^3x_5 (x_1 x_{12} x_{13} x_{34} x_{35})^{-\gamma}$	= 31.684
	$K_{5e} = \left(\frac{3}{4\pi}\right)^5 \int_0^1 d^3x_1 \ldots \int_0^1 d^3x_5 (x_1 x_{12} x_{23} x_{24} x_{25})^{-\gamma}$	= 28.883
	$K_{5f} = \left(\frac{3}{4\pi}\right)^5 \int_0^1 d^3x_1 \ldots \int_0^1 d^3x_5 (x_1 x_{12} x_{23} x_{14} x_{45})^{-\gamma}$	= 30.723
	$K_{5g} = \left(\frac{3}{4\pi}\right)^5 \int_0^1 d^3x_1 \ldots \int_0^1 d^3x_5 (x_1 x_{12} x_{23} x_{34} x_{35})^{-\gamma}$	= 27.800
	$K_{5h} = \left(\frac{3}{4\pi}\right)^5 \int_0^1 d^3x_1 \ldots \int_0^1 d^3x_5 (x_1 x_{12} x_{13} x_{34} x_{45})^{-\gamma}$	= 30.328
	$K_{5i} = \left(\frac{3}{4\pi}\right)^5 \int_0^1 d^3x_1 \ldots \int_0^1 d^3x_5 (x_1 x_{12} x_{23} x_{34} x_{45})^{-\gamma}$	= 27.204

NOTES.—Coefficients entering the combinations (A10), (A13), and (A16) of hierarchical amplitudes. They have been evaluated, for $\gamma = 1.71$, by means of a Monte Carlo multiple integration.

In the right-hand side of equation (A11) the first contribution comes from *star graphs*, while the last one comes from *snake graphs*. The middle term takes into account the presence of one differently *rooted* tree. In this case, too, we substitute equation (A11) in equation (4.7) and obtain the fourth *moment* of the mass distribution:

$$R_{4,k} = \left[Q_{5,1}\left(1 + 4\,\frac{K_{4a}}{K_1^4}\right) + 12 Q_{5,2}\left(\frac{K_2}{K_1^2} + \frac{K_{3b}}{K_1^3} + \frac{K_{4b}}{K_1^4} + 2\,\frac{K_{4c}}{K_1^4}\right) + 12 Q_{5,3}\left(\frac{K_2^2}{K_1^4} + 2\,\frac{K_{3a}}{K_1^3} + 2\,\frac{K_{4d}}{K_1^4}\right)\right]. \tag{A12}$$

The four K_4 quantities come from the quadruple volume integration occurring in the computation of $\langle M^4 \rangle_k$. Their full expressions and numerical values are reported in Table 5. Following the same pattern as in the previous subsections, we compare equation (A12) with observational data. In this case the combination of the Q_5's reads

$$Q_{5,1} + 11.43 Q_{5,2} + 9.90 Q_{5,3} = 0.675 \pm 0.107\,. \tag{A13}$$

Equation (A13) is relevant because it represents one of the very first pieces of information on fifth-order correlation. Inded, there is strong evidence for the hierarchical pattern to hold up to the fifth order, with a $\sim 6\,\sigma$ signal.

4. ANALYSIS OF THE SIX-POINT FUNCTION

The growth of the number of terms to be added in equation (4.2) leads us to consider, for $n = 6$, contributions from six different *trees* and 1296 total terms. Then, the expression of the six-point correlation function is

$$\begin{aligned}\xi^{(5)}_{0\ldots5} = {} & Q_{6,1}[\xi_{01}\,\xi_{02}\,\xi_{03}\,\xi_{04}\,\xi_{05} + \cdots \text{(6 terms)}] \\ & + Q_{6,2}[\xi_{01}\,\xi_{12}\,\xi_{23}\,\xi_{24}\,\xi_{25} + \cdots \text{(120 terms)}] \\ & + Q_{6,3}[\xi_{01}\,\xi_{12}\,\xi_{13}\,\xi_{34}\,\xi_{35} + \cdots \text{(90 terms)}] \\ & + Q_{6,4}[\xi_{01}\,\xi_{12}\,\xi_{23}\,\xi_{24}\,\xi_{45} + \cdots \text{(360 terms)}] \\ & + Q_{6,5}[\xi_{01}\,\xi_{12}\,\xi_{23}\,\xi_{34}\,\xi_{35} + \cdots \text{(360 terms)}] \\ & + Q_{6,6}[\xi_{01}\,\xi_{12}\,\xi_{23}\,\xi_{34}\,\xi_{45} + \cdots \text{(360 terms)}] \,. \end{aligned} \tag{A14}$$

Due to the complexity of this expression, the form of the fifth moment of the mass distribution looks rather unpleasant. In fact,

$$\begin{aligned} R_{5,k} = {} & Q_{6,1}\left(1 + 5\,\frac{K_{5a}}{K_1^5}\right) + 20Q_{6,2}\left(\frac{K_2}{K_1^2} + \frac{K_{4a}}{K_1^4} + \frac{K_{5b}}{K_1^5} + 3\,\frac{K_{5c}}{K_1^5}\right) + 30Q_{6,3}\left(\frac{K_{3b}}{K_1^3} + 2\,\frac{K_{5d}}{K_1^5}\right) + 60Q_{6,4}\left(\frac{K_2^2}{K_1^4} + 2\,\frac{K_{4c}}{K_1^4} + 2\,\frac{K_{5e}}{K_1^5} + \frac{K_{5f}}{K_1^5}\right) \\ & + 60Q_{6,5}\left(\frac{K_{3a}}{K_1^3} + \frac{K_2\,K_{3b}}{K_1^5} + \frac{K_{4d}}{K_1^4} + \frac{K_{5g}}{K_1^5} + 2\,\frac{K_{5h}}{K_1^5}\right) + 120Q_{6,6}\left(\frac{K_2\,K_{3a}}{K_1^5} + \frac{K_{4d}}{K_1^4} + \frac{K_{5i}}{K_1^5}\right). \end{aligned} \tag{A15}$$

Expressions and numerical values of the K_5 coefficients are given in Table 5.

By fitting the data on central moments to equation (A15), we get

$$Q_{6,1} + 18.06Q_{6,2} + 13.79Q_{6,3} + 49.50Q_{6,4} + 47.96Q_{6,5} + 43.59Q_{6,6} = 0.44 \pm 0.12 \,. \tag{A16}$$

Similarly to equation (A13), equation (A16) is important in view of the paucity of data on sixth-order correlation. In this case, again, the hierarchical pattern shows up with a 4 σ signal.

REFERENCES

Balian, R., & Schaeffer, R. 1989a, A&A, 220, 1
———. 1989b, A&A, 226, 373
Bardeen, J. M., Bond, J. R., Kaiser, N., & Szalay, A. S. 1986, ApJ, 304, 15
Begeman, K. 1988, Ph.D. thesis, Groningen
Blumenthal, G. R., Faber, S. M., Primack, J. R., & Rees, M. J. 1984, Nature, 311, 517
Bonometto, S. A., Borgani, S., Persic, M., & Salucci, P. 1990, ApJ, 356, 350
Borgani, S., & Bonometto, S. A. 1990, ApJ, 348, 398
Bosma, A. 1981, AJ, 86, 1825
Carignan, C., & Freeman, K. C. 1988, ApJ, 332, L33
Carignan, C., Sancisi, R., & van Albada, T. S. 1988, AJ, 95, 37
Davis, M., Efstathiou, G., Frenk, C. S., & White, S. D. M. 1985, ApJ, 292, 371
Davis, M., & Peebles, P. J. E. 1977, ApJS, 34, 425
Dekel, A., & Rees, M. J. 1987, Nature, 326, 455
de Lapparent, V., Geller, M. J., & Huchra, J. P. 1987, in 13th Texas Symposium on Relativistic Astrophysics, ed. M. P. Ulmer (Singapore: World Scientific), 281
Efstathiou, G., Frenk, C. S., White, S. D. M., & Davis, M. 1988, MNRAS, 235, 715
Einasto, J., Klypin, A., & Saar, E. 1986, MNRAS, 219, 457
Faber, S. M., & Gallagher, J. S. 1979, ARA&A, 17, 135
Freeman, K. C. 1970, ApJ, 160, 811
Fry, J. N. 1982, ApJ, 262, 424
———. 1984a, ApJ, 277, L5
———. 1984b, ApJ, 279, 499
Fry, J. N., & Peebles, P. J. E. 1978, ApJ, 221, 19
Geller, M. J. 1987, in Large Scale Structure in the Universe, Proc. of the SAAS-FEE School, ed. L. Martinet & M. Mayor (Geneva: Geneva Observatory), 71
Gott III, J. R., & Turner, E. L. 1979, ApJ, 232, L79
Groth, E. J., & Peebles, P. J. E. 1977, ApJ, 217, 385
Hamilton, A. J. S. 1988, ApJ, 332, 67
Jensen, L. G., & Szalay, A. S. 1986, ApJ, 305, L5
Kaiser, N. 1984, ApJ, 284, L9
Lake, G., & Tremaine, S. 1980, ApJ, 239, L13
Maddox, S. J., Efstathiou, G., Sutherland, W. J., & Loveday, J. 1990, MNRAS, 242, 43
Peebles, P. J. E. 1980, The Large Scale Structure of the Universe (Princeton: Princeton University Press)
———. 1986, Nature, 321, 27
Peebles, P. J. E., & Groth, E. J. 1975, ApJ, 196, 1
Persic, M., & Salucci, P. 1988, MNRAS, 234, 131
———. 1990a, MNRAS, 245, 577
———. 1990b, ApJ, 355, 44
———. 1991, ApJ, 368, 60
Politzer, D., & Wise, M. 1984, ApJ, 285, L1
Riordan, J. 1958, An Introduction to Combinatorial Analysis, (New York: Wiley)
Rubin, V. C., Burstein, D., Ford, W. K., Jr., & Thonnard, N. 1985, ApJ, 289, 81
Seldner, M., Siebers, B., Groth, E. J., & Peebles, P. J. E. 1977, AJ, 82, 249
Shane, C. D., & Wirtanen, C. A. 1967, Pub. Lick Obs., 22
Sharp, N. A., Bonometto, S. A., & Lucchin, F. 1984, A&A, 130, 79
Szapudi, I., Szalay, A. S., & Boschan, P. 1989, PASP, in press
Valdarnini, R., & Borgani, S. 1990, MNRAS, submitted
van der Kruit, P. C. 1987, A&A, 173, 59